Charge Transfer

International Edition: DOI: 10.1002/anie.201806093
German Edition: DOI: 10.1002/ange.201806093

Tunable Chiroptical Properties from the Plasmonic Band to Metal–Ligand Charge Transfer Band of Cysteine-Capped Molybdenum Oxide Nanoparticles

Yiwen Li[+], Jiaji Cheng[+], Jiagen Li, Xi Zhu, Tingchao He, Rui Chen,* and Zikang Tang**

Abstract: *Understanding the interactions between a semiconducting nanocrystal surface and chiral anchoring molecules could resolve the mechanism of chirality induction in nanoscale and facilitate the rational design of chiral semiconducting materials for chiroptics. Now, chiral molybdenum oxide nanoparticles are presented in which chirality is transferred via a bio-to-nano approach. With facile control of the amount of chiral cysteine molecules under redox treatment, circular dichroism (CD) signals are generated in the plasmon region and metal–ligand charge-transfer band. The obtained enhanced CD signals with tunable lineshapes illustrate the possibility of using chiral molybdenum oxide nanoparticles as potentials for chiral semiconductor nanosensors, optoelectronics, and photocatalysts.*

Chiral inorganic nanocrystals (NCs) as an emerging area has revolutionized the motif of chirality, which was originally derived from stereochemistry since the first observation of optical activity in quartz by F. J. D. Arago.[1] Nowadays, attentions on the synthesis of chiral inorganic NCs are further extended on enhanced chiroptical effects, chirogenesis and potentials in which chiral inorganic NCs could provide to interdisciplinary fields such as optical and biosensing,[2] chiral recognitions[3] and polarization-based display devices.[4] Intuitively, chiral inorganic NCs with chirality transferred from chiral ligands that are bound to their surface are commonly studied, and the species of inorganic materials can vary from metallic nanoparticles (NPs) or clusters to a variety of semiconductor NCs.[5]

Among them, chiral metal oxide NPs with ligand induced chirality has triggered tremendous interests for their essential applications in chiral catalysis, biomaterials, optics and understanding of light–matter interactions. To date, Y. Gun'ko and coauthors[6] reported that diphenylethylenediamine-capped TiO_2 NPs can express chiroptical activities at their band-edge region owing to the overlap of the chiral ligand highest-occupied molecular orbital (HOMOs) with the TiO_2 quantum-dot valence-band states. More recently, J. Yeom et al.[7] synthesized Co_3O_4 chiromagnetic NPs and their gels that can be used for real-time magnetic field modulation. These NCs with chiral distortions of the crystal lattices caused by the chiral ligands (cysteine) exhibited enhanced chiroptical activity in the visible range, suggesting that metal oxide NPs with structural chirality and magnetism can be expanded to a wide range of nanomaterials with tunable chiroptical and chiral magnetic properties. Further, doped semiconductor metal oxide can also provide a versatile platform for obtaining chiral nanostructures with tunable extinction behaviors which can be modulated by changing carrier concentration through chemical doping.[8] Kotov and colleagues,[9] for example, synthesized chiral WO_{3-x} NPs via a bio-to-nano chirality transfer approach. By capping the WO_{3-x} NCs by aspartic acid (Asp) and proline (Pro) molecules, the amino acids are attached to the NP surface through C-O-W linkages and weakly coordinated to the NP surface. Thanks to the metal-to-ligand charge transfer (MLCT) effect, they successfully observed an unusual chiroelectronic band at visible region and a chiroplasmonic signal at near infrared (NIR) region. When the capping chiral molecules are different, the chiroptical responses also varied because the molecular binding mode of the two amino acids to the NP surface are different where Asp has one additional C-O-W linkage compared to Pro resulting in stronger distortion of the inorganic crystal lattice and greater intensity of circular dichroism (CD) bands.

In light of the strong CD activities of chiral WO_{3-x} NPs through MLCT effect, herein, we present chiral MoO_{3-x} and MoO_2 NPs with tunable absorption properties by a one-pot synthesis in which the chiral cysteine molecules serve as both reducing and capping agent in aqueous solution. The obtained sub-stoichiometric chiral MoO_{3-x} NPs exhibit a strong relationship between the amount of chiral cysteine ligand used for reaction and chiroptical activities at surface plasmon resonance (SPR) band and MLCT band region. Owing to the strong Mo–S bond (even stronger than a typical C-O-W linkage mentioned above), the highest anisotropic g-factor of

[*] Y. Li,[+] Prof. R. Chen
Department of Electrical and Electronic Engineering
Southern University of Science and Technology
Shenzhen, 518055 (P. R. China)
E-mail: chen.r@sustc.edu.cn
Dr. J. Cheng,[+] Prof. T. He
College of Physics and Energy, Shenzhen University
Shenzhen 518060 (P. R. China)
E-mail: tche@szu.edu.cn
Y. Li,[+] Prof. Z. Tang
The Institute of Applied Physics and Materials Engineering
University of Macau
Avenida da Universidade, Taipa (Macau)
E-mail: zikang@umac.mo
J. Li, Prof. X. Zhu
School of Science and Engineering
The Chinese University of Hong Kong
Shenzhen (P. R. China)
[+] These authors contributed equally to this work.
Supporting information and the ORCID identification number(s) for the author(s) of this article can be found under: https://doi.org/10.1002/anie.201806093.

such a system can reach about $7X10^{-3}$, which is more than four times higher than the chiral WO_{3-x} system capping by Asp or Pro molecules. Further, the chiral origin of such system is confirmed by time-dependent density functional theory (TDDFT) simulations. It was found that the electronic state interactions caused by orbital couplings between the chiral ligands and NPs are vital for the induction of chirality. Such tunable chiroptical activities of molybdenum oxide will create a unique pathway for the development of chiroptics, plasmonic sensing, and biomedicine.

The aqueous chiral molybdenum oxide NPs capped with L- or D-cysteine molecules were prepared through the facile one-step self-assembling synthesis through the bulk MoS_2 powder sources. In the synthesis process, the cysteine molecules serve as both capping agent and reducing agent simultaneously as detailed in the Supporting Information. Figure 1 a illustrates the processes of H_2O_2 oxidation and the formation of small nanodots. TEM characterization demonstrates that the average size of pristine MoO_3 NPs is around 3 nm (Supporting Information, Figure S2). Furthermore, different amount of cysteine could result in chiral oxide NPs with different colors. After redox treatment with cysteine, we select 5, 20, and 60 mg cysteine-capped oxide NPs with typical blue, green, and brown color to characterize their morphology. Figure 1 b,c show the 5 and 20 mg treated NPs possess similar size distribution (ca. 3 nm), which is consistent to the size of pristine MoO_3 NPs. However, the 60 mg cysteine capped NPs exhibits larger NPs (ca. 29 nm; Figure 1 d). Figure 1 f,g indicate that the L- and D-Cys can induce similar color change tendency, that is, from blue, green, to brown, which correspond to a small, moderate, and large amount of capping ligand, respectively. Figure 1 e shows the high-resolution TEM image of 20 mg L-Cys treated sample, in which the lattice spacing corresponds (123) crystal plane of MoO_{3-x}.

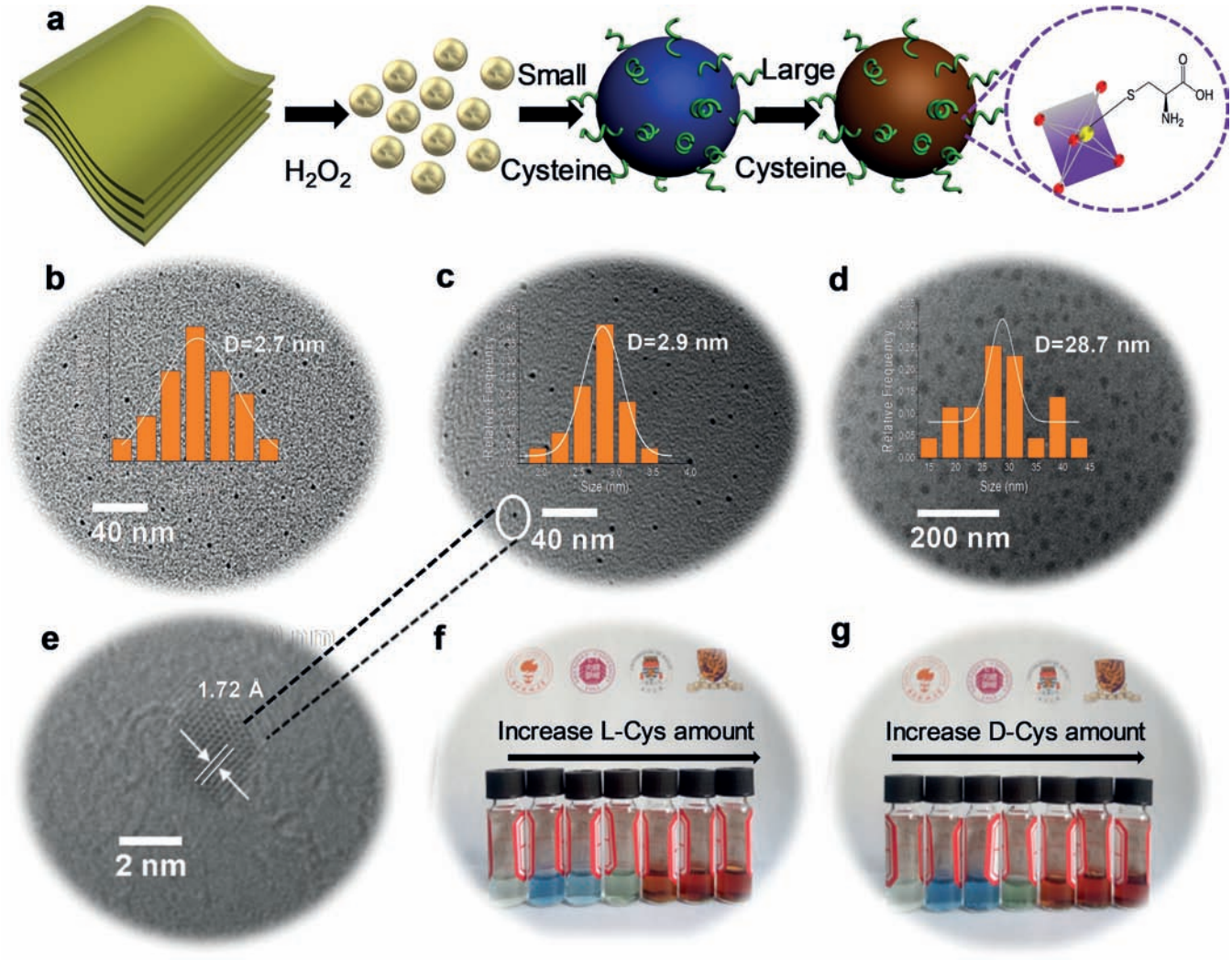

Figure 1. Fabrication of chiral cysteine-capped molybdenum oxide NPs associated with morphology characterization. a) Illustration of the synthesis of chiral NPs. The dark yellow flake is MoS_2, which is oxidized by H_2O_2 to form MoO_3 nanodots (ivory sphere). The different amount of cysteine could reduce the MoO_3 to obtain various cationic valence (blue sphere MoO_{3-x}, brown MoO_2, green ligand is L- or D-cysteine). b)–d) TEM images and size distribution of 5 mg, 20 mg, and 60 mg L-Cys capped chiral NPs, respectively. f) HRTEM image of 20 mg L-Cys capped chiral NPs. e),g) Photographs of different amount of L- and D-cysteine treated NPs, which from left to right corresponds 0, 5, 10, 20, 40, 60, 80 mg cysteine dispersed in 1.5 mL solution, respectively.

The X-ray surface photoelectron spectrum (XPS) results indicate that the molybdenum element valence could decrease from Mo^{VI} to Mo^{IV} during reduction reaction progressively (Figure 2). The as-prepared pristine MoO_3 exhibits pure Mo^{VI} element in NPs. The two apparent blue peaks located at 233.35 eV and 236.55 eV correspond to Mo $3d_{5/2}$ and Mo $3d_{3/2}$ orbitals. For the blue color solution with 5 mg L-Cys, the XPS results shows that there are mixed valences between Mo^{VI} (blue peaks) and Mo^{V} (orange peaks). The peaks located at 231.95 eV and 235.10 eV correspond to the Mo^{V} $3d_{5/2}$ and $3d_{3/2}$ orbitals. With continuous redox reaction, the green solution sample (20 mg L-Cys capped NPs) possess mixed valences involving Mo^{VI} and Mo^{IV}, and the light green peak indicate the Mo^{IV} $3d_{5/2}$ orbital at 229.1 eV. For the brown solution (60 mg L-Cys capped NPs), the Mo^{VI} and Mo^{V} totally vanished while the pure Mo^{IV} orbitals appear at 229.1 eV and 232.2 eV, which demonstrates that the MoO_2 NPs are formed. The larger size of MoO_2 NPs (ca. 20 nm) could be explained by the aggregation of MoO_2 caused by weak solubility in water as confirmed by the TEM observation (Figure 1 d). The XPS results of MoO_2 NPs exhibit the excessive S element from cysteine (Supporting Information, Figure S3). Deconvolution and calculation of relative peak areas ratio show that the ratio of Mo^{VI} to Mo^{V} is 1.875 for the 5 mg L-Cys capped NPs, and the sub-stoichiometric oxides could be expressed as $MoO_{2.83}$. Furthermore, the 20 mg L-Cys capped NPs can be expressed as $MoO_{2.68}$ according to the ratio of Mo^{VI} to Mo^{IV} (ca. 2.25). The abovementioned results present the cysteine could reduce the MoO_3 step by step and produce NPs with different valences, which is similar to the $NaBH_4$ reduction effect.[10]

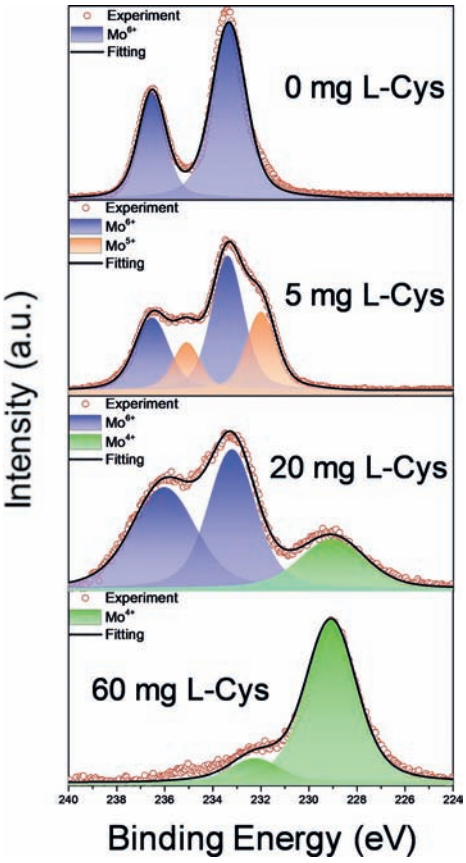

Figure 2. XPS spectra of different L-Cys capped NPs with deconvoluted Mo 3d peaks. Blue, orange, and green peak areas corresponds to three valence states of molybdenum with Mo^{VI}, Mo^{V}, and Mo^{IV} respectively.

The UV/Vis and CD spectra were then utilized to investigate the chiroptical activity of L- and D-Cys capped MoO_{3-x} and MoO_2. The absorption spectra clearly reveal that the surface plasmonic peak and MLCT peak could be tuned via the adjustment of capping ligand concentration (Figure 3 b). With the addition of small amount of L- or D-Cys, the MoO_{3-x} NPs exhibit only strong NIR absorption band at around 823 nm. The plasmonic induced absorption peak also indicates refractive index dependent through solvents with various refractive indices exchange for the 5 mg L-Cys capped NPs (Supporting Information, Figure S4). For the 20 mg L-Cys capped NPs with mixed Mo^{VI} and Mo^{IV}, the plasmonic band intensity decrease along with the appearance of a weak absorption shoulder in the visible region. It indicates the MLCT absorption could relate to the Mo^{IV} complex directly. For the completed reduction to MoO_2 NPs, the absorption spectra exhibit strong MLCT induced visible absorption band and the plasmonic peak completely disappeared. The reason is due to the absence of necessary carrier density that can result in plasmonic frequency in MoO_2 compared to MoO_{3-x} NPs. The detailed fundamental background of transition is discussed in the Supporting Information. Their chiroptical properties display close relation with their absorption peak position. The pristine MoO_3 NPs show silent chiral activity without chiral ligand capping (Supporting Information, Figure S5). Figure 3 a shows the CD spectra of both L- and D-Cys capped NPs with ligand amount range from 5 to 80 mg. L- and D-Cys capped NPs reveal strong mirror-image CD spectra for all samples. For the small amount cysteine modified NPs, the chiral signals only emerge in the NIR region, which correspond to the plasmonic absorption. For the 5 mg cysteine capped NPs, the CD ellipticity is smaller than 5 mdeg and the relevant g-factor values is in the order of 10^{-4} (Figure 3 e,f), which are comparable to the previous chiral-ligand-capped plasmonic metallic NPs.[11] However, with the continuous increase of cysteine, the chiroplasmonic band disappears along with the CD signals emerged at visible region. Meanwhile, CD ellipticities are measured to 160 and 300 mdeg for 40 and 60 mg cysteine capped NPs, respectively. As a consequence, the largest g-factor value can be up to $7 X10^{-3}$ (Figure 3 c). The g-factor values of CD signal at 580 nm as a function of cysteine amount is summarized in Figure 3 d. The g-factor value saturates when the ligand amount is larger than 60 mg. The strong coordinative bond between Mo and S atoms may contribute to the larger values of g-factor compared with other chiral non-thiol ligands. Among all the samples, the 20 mg cysteine-capped NCs possess both plasmonic and MLCT transition absorption, nevertheless it only displays weak visible CD signal with a g-factor value of $5 X 10^{-4}$. Their chiroptical responses in NIR plasmonic region are absent. It may be due to the low loading of MoO_{3-x} NPs and inefficient ligand chiral transfer in plasmonic dipole.[12] Based on this issue, we have investigated the chiroptical properties of their sediment after centrifugation. The precipitated productions were dispersed in deionized water. There is no

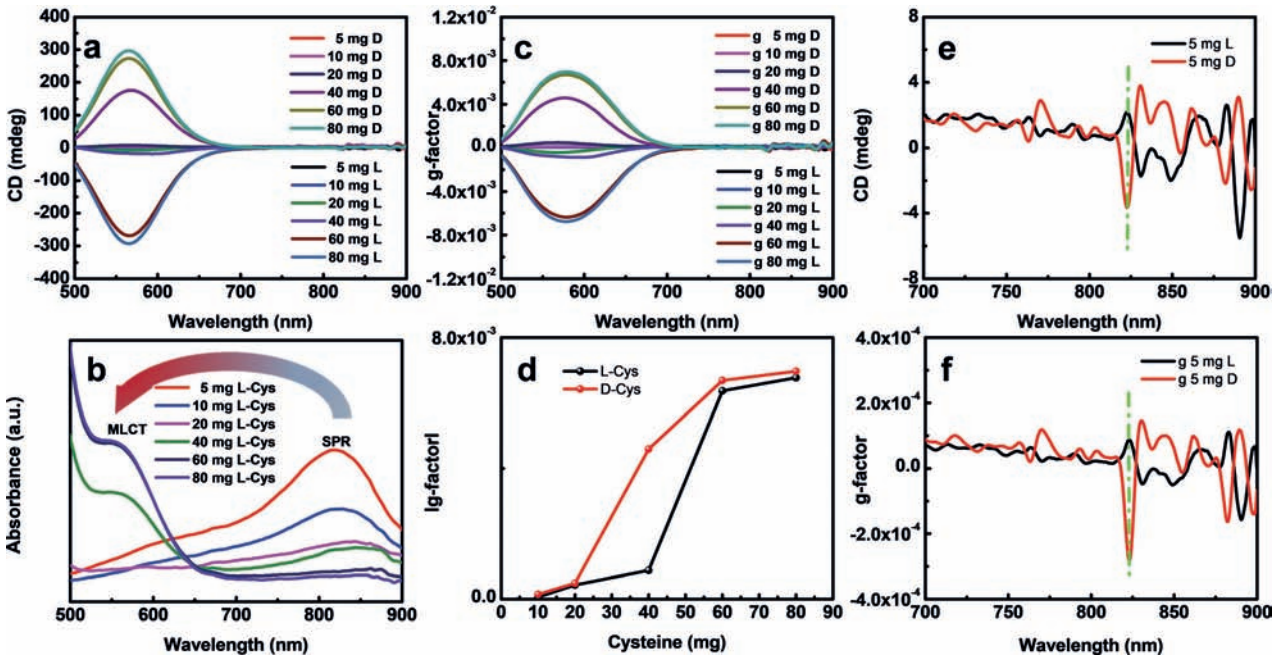

Figure 3. Chiroptical activity observation of L- and D-Cys-capped NPs. a) CD spectra, b) absorption spectra, c) g-factor spectra of different amount of both L- and D-Cys capped NPs. d) g-factor value for 580 nm CD signal as a function of cysteine amount. e),f) CD and g-factor spectra of 5 mg L- and D-Cys capped NPs in NIR region.

obvious change in CD peak position for the 5 and 60 mg cysteine capped NPs, but the NPs capped by 20 mg cysteine display weak CD activity again in plasmonic band (Supporting Information, Figures S7–S9). It could be explained that the plasmonic transition dominates in colloid NPs but MLCT dominates in the supernatant complex. It should be noted that chiroptical activities of all sediment decrease dramatically compared to the as-prepared NPs solution. The main ligands in supernatant fraction that induce strong MLCT absorption suffer from damage after centrifugation. After precipitation treatment, the 20 mg cysteine-capped NPs shows much weaker CD signal in the MLCT band with unchanged peak position (ca. 580 nm) and a relatively small g-factor value (ca. $1 X10^{-4}$). All the samples display much weaker CD activity in MLCT transition band compared with as-prepared samples. The g-factors of sediment as a function of cysteine amount have been summarized (Supporting Information, Figure S10).

To investigate the original derivation of chiral behavior, we performed the simulation and predicted their chiroptical properties via TDDFT method,[13] details are shown in the Supporting Information. Mo_4O_8 nanoclusters were selected as the smallest meaningful model structure for chiral oxides. Four chiral ligands were functionalized to the nanocluster. The initial and optimized structures of molybdenum oxide cluster with both L- and D-cysteine were shown in the Supporting Information, Figure S11 and Figure 4 a,b, respectively. Figure 4 c–d demonstrates that the calculated absorption and CD spectra of L- and D-Cys capped nanocluster complexes. Because of the much smaller size of simulated cluster compared with the actual oxides NPs, the simulated absorption and CD spectra exhibit a blue-shift of 150 nm for MLCT band with respect to our experimental results. The observed chiral signals keep consistent with absorption region and display mirror-image spectra for L- and D-Cys capped nanocluster complexes, confirming the strong interaction between nanocluster and chiral molecules. The MLCT band transition is contributed by the transition from the metal-δ orbitals complexing ligand-based π orbitals associated with the HOMO and ligand-based π* orbitals associated with the LUMO. The delocalized HOMO, HOMO−1, HOMO−2 orbitals of nanocluster complex both in Mo_4O_8 and cysteine indicates that strong hybridization of orbital coupling between orbital wavefunction of the chiral ligand and HOMO electronic states of nanocluster. The chiroptical transfer from molecular to nanocluster is therefore due to the coupling of electronic states, which is similar to the orbital interactions in other semiconductor NCs (Supporting Information, Figure S13).[5c,14]

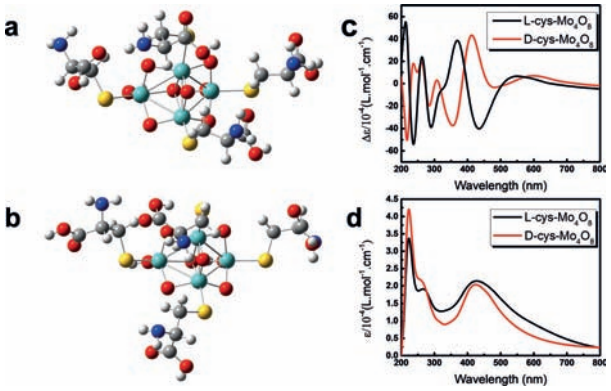

Figure 4. TDDFT simulation for cysteine capped Mo_4O_8 nanocluster. a) L- and b) The optimized structure of the D-Cys-nanocluster. c) Calculated CD spectra and d) absorption spectra for both L- and D-capped nanocluster.

In summary, the cysteine capped molybdenum oxides NPs were successfully prepared by a one-step redox process. Based on XPS analytical analysis, it was found that the chiral cysteine capping ligand could alternatively serve as reductive agent to mediate cationic valence depending on cysteine amount. Our investigation suggests that chiroptical properties of chiral NPs could be tuned as a function of cysteine amount from the plasmonic band to metal–ligand charge transfer band. Furthermore, the strong chirality with a g-factor value of about $7 X10^{-3}$ is achieved in MLCT band in visible region. The chiral transfer from ligand to NPs were studied and discussed in term of the electronic state coupling, with the help of TDDFT simulation method. This work sheds light on the future potential chiroptical application in molybdenum oxides NPs to achieve dynamics tunable and fully cover spectra of chiral response.

Acknowledgements

This work is supported by National Natural Science Foundation of China (11574130 and 11404161), Shenzhen Science and Technology Innovation Committee (Projects Nos.: KQJSCX20170726145748464, JCYJ20150930160634263, JCYJ20170302142433007, and KQTD2015071710313656), and the research and development grant funding from University of Macau (MYRG 2018-00142, FDCT 199/2017/A3). R.C. acknowledges the support from National 1000 plan for Young Talents.

Conflict of interest

The authors declare no conflict of interest.

Keywords: chiroptics · metal–ligand charge transfer · molybdenum oxide · nanoparticles · surface plasmon

How to cite: *Angew. Chem. Int. Ed.* **2018**, *57*, 10236–10240
Angew. Chem. **2018**, *130*, 10393–10397

[1] L. D. Barron, D. A. Long, *Molecular light scattering and optical activity*, Cambridge University Press, Cambridge, **2004**.

[2] a) X. Wu, L. Xu, L. Liu, W. Ma, H. Yin, H. Kuang, L. Wang, C. Xu, N. A. Kotov, *J. Am. Chem. Soc.* **2013**, *135*, 18629–18636; b) W. Ma, M. Sun, P. Fu, S. Li, L. Xu, H. Kuang, C. Xu, *Adv. Mater.* **2017**, *29*, 1703410; c) W. Ma, H. Kuang, L. Xu, L. Ding, C. Xu, L. Wang, N. A. Kotov, *Nat. Commun.* **2013**, *4*, 2689; d) Z. Y. Bao, W. Zhang, Y. L. Zhang, J. He, J. Dai, C. T. Yeung, G. L. Law, D. Y. Lei, *Angew. Chem. Int. Ed.* **2017**, *56*, 1283; *Angew. Chem.* **2017**, *129*, 1303.

[3] a) M. Sun, L. Xu, J. H. Banhg, H. Kuang, S. Alben, N. A. Kotov, C. Xu, *Nat. Commun.* **2017**, *8*, 1847; b) A. Kghnle, T. R. Linderoth, B. R. Hammer, F. Besenbacher, *Nature* **2002**, *415*, 891–893; c) R. Mckendry, M. E. Theoclitou, T. Rayment, C. Abell, *Nature* **1998**, *391*, 566–568; d) M. V. Mukhina, I. V. Korsakov, V. G. Maslov, P. M. Finn, G. Joseph, A. V. Baranov, A. V. Fedorov, Y. K. Gun'Ko, *Sci. Rep.* **2016**, *6*, 24177.

[4] a) J. E. Govan, E. Jan, A. Querejeta, N. A. Kotov, Y. K. Gun'Ko, *Chem. Commun.* **2010**, *46*, 6072–6074; b) J. Ahn, E. Lee, J. Tan, W. Yang, B. Kim, J. Moon, *Mater. Horiz.* **2017**, *4*, 851; c) Y. Shi, P. Duan, S. Huo, Y. Li, M. Liu, *Adv. Mater.* **2018**, *30*, 1705011.

[5] a) W. Ma, L. Xu, A. F. de Moura, X. Wu, H. Kuang, C. Xu, N. A. Kotov, *Chem. Rev.* **2017**, *117*, 8041; b) J. Cheng, E. H. Hill, Y. Zheng, T. He, Y. Liu, *Mater. Chem. Front.* **2018**, *2*, 662–678; c) A. Ben-Moshe, B. M. Maoz, A. O. Govorov, G. Markovich, *Chem. Soc. Rev.* **2013**, *42*, 7028–7041; d) X. Wang, Z. Tang, *Small* **2017**, *13*, 1601115; e) X. Gao, X. Zhang, K. Deng, B. Han, L. Zhao, M. Wu, L. Shi, J. Lv, Z. Tang, *J. Am. Chem. Soc.* **2017**, *139*, 8734–8739; f) J. Kumar, K. G. Thomas, L. M. Lizmarz#n, *Chem. Commun.* **2016**, *52*, 12555–12569; g) T. He, J. Li, X. Li, C. Ren, Y. Luo, F. Zhao, R. Chen, X. Lin, J. Zhang, *Appl. Phys. Lett.* **2017**, *111*, 151102; h) B. Leah, H. Torsten, *ChemNanoMat* **2017**, *3*, 841–841; i) I. Dolamic, S. Knoppe, A. Dass, T. Bgrgi, *Nat. Commun.* **2012**, *3*, 798.

[6] O. Cleary, F. Purcell-Milton, A. Vandekerckhove, Y. K. Gun′Ko, *Adv. Opt. Mater.* **2017**, *5*, 1601000.

[7] J. Yeom, U. S. Santos, M. Chekini, M. Cha, A. M. De, N. A. Kotov, *Science* **2018**, *359*, 309–314.

[8] P. Yin, Y. Tan, H. Fang, M. Hegde, P. V. Radovanovic, *Nat. Nanotechnol.* **2018**, *13*, 463–467.

[9] S. Jiang, M. Chekini, Z.-B. Qu, Y. Wang, A. Yeltik, Y. Liu, A. Kotlyar, T. Zhang, B. Li, H. V. Demir, N. A. Kotov, *J. Am. Chem. Soc.* **2017**, *139*, 13701–13712.

[10] Y. Li, J. Cheng, Y. Liu, P. Liu, W. Cao, T. He, R. Chen, Z. Tang, *J. Phys. Chem. C* **2017**, *121*, 5208–5214.

[11] a) G. Shemer, O. Krichevski, G. Markovich, T. Molotsky, I. Lubitz, A. B. Kotlyar, *J. Am. Chem. Soc.* **2006**, *128*, 11006–11007; b) W. Chen, A. Bian, A. Agarwal, L. Liu, H. Shen, L. Wang, C. Xu, N. A. Kotov, *Nano Lett.* **2009**, *9*, 2153–2159; c) J. Cheng, G. Le Saux, J. Gao, T. Buffeteau, Y. Battie, P. Barois, V. Ponsinet, M.-H. Delville, O. Ersen, E. Pouget, R. Oda, *ACS Nano* **2017**, *11*, 3806–3818.

[12] Z. Fan, A. O. Govorov, *Nano Lett.* **2010**, *10*, 2580–2587.

[13] a) U. Tohgha, K. K. Deol, A. G. Porter, S. G. Bartko, J. K. Choi, B. M. Leonard, K. Varga, J. Kubelka, G. Muller, M. Balaz, *ACS Nano* **2013**, *7*, 11094–11102; b) K. Varga, S. Tannir, B. E. Haynie, B. M. Leonard, S. V. Dzyuba, J. Kubelka, M. Balaz, *ACS Nano* **2017**, *11*, 9846–9853; c) R. A. Gaussian09, M. J. Frisch, G. W. Trucks, H. B. Schlegel, G. E. Scuseria, M. A. Robb, J. R. Cheeseman, G. Scalmani, V. Barone, G. A. Petersson, H. Nakatsuji, X. Li, M. Caricato, A. Marenich, J. Bloino, B. G. Janesko, R. Gomperts, B. Mennucci, H. P. Hratchian, J. V. Ortiz, A. F. Izmaylov, J. L. Sonnenberg, D. Williams-Young, F. Ding, F. Lipparini, F. Egidi, J. Goings, B. Peng, A. Petrone, T. Henderson, D. Ranasinghe, V. G. Zakrzewski, J. Gao, N. Rega, G. Zheng, W. Liang, M. Hada, M. Ehara, K. Toyota, R. Fukuda, J. Hasegawa, M. Ishida, T. Nakajima, Y. Honda, O. Kitao, H. Nakai, T. Vreven, K. Throssell, J. A. Montgomery, Jr., J. E. Peralta, F. Ogliaro, M. Bearpark, J. J. Heyd, E. Brothers, K. N. Kudin, V. N. Staroverov, T. Keith, R. Kobayashi, J. Normand, K. Raghavachari, A. Rendell, J. C. Burant, S. S. Iyengar, J. Tomasi, M. Cossi, J. M. Millam, M. Klene, C. Adamo, R. Cammi, J. W. Ochterski, R. L. Martin, K. Morokuma, O. Farkas, J. B. Foresman, and D. J. Fox, Gaussian, Inc., Wallingford CT, **2016**.

[14] a) J. K. Choi, B. E. Haynie, U. Tohgha, L. Pap, K. W. Elliott, B. M. Leonard, S. V. Dzyuba, K. Varga, J. Kubelka, M. Balaz, *ACS Nano* **2016**, *10*, 3809–3815; b) M. T. Frederick, V. A. Amin, E. A. Weiss, *J. Phys. Chem. Lett.* **2013**, *4*, 634–640; c) M. T. Frederick, E. A. Weiss, *ACS Nano* **2010**, *4*, 3195–3200; d) J. Cheng, J. Hao, H. Liu, J. Li, J. Li, X. Zhu, X. Lin, K. Wang, T. He, *ACS Nano* **2018**, *12*, 5341–5350.

Manuscript received: June 1, 2018
Revised manuscript received: June 21, 2018
Accepted manuscript online: June 25, 2018
Version of record online: July 9, 2018

